Sub-barrier fusion in the ^{37}Cl + ^{130}Te system

Rudra N. Sahoo,[1,*] Malika Kaushik,[1] Arshiya Sood,[1] Pawan Kumar,[1] Arzoo Sharma,[1] Swati Thakur,[1] Pushpendra P. Singh,[1,†] P. K. Raina,[1] Md. Moin Shaikh,[2] Rohan Biswas,[3] Abhishek Yadav,[3] J. Gehlot,[3] S. Nath,[3] N. Madhavan,[3] V. Srivastava,[4] Manoj K. Sharma,[5] B. P. Singh,[6] R. Prasad,[6] Anjali Rani,[7] A. Banerjee,[7] Unnati Gupta,[7] Nabendu K. Deb,[8] and B. J. Roy[9]

[1]*Department of Physics, Indian Institute of Technology Ropar, Rupnagar 140 001, Punjab, India*
[2]*Variable Energy Cyclotron Centre, 1/AF, Bidhannagar, Kolkata 700 064, India*
[3]*Nuclear Physics Group, Inter-University Accelerator Centre, New Delhi 110 067, India*
[4]*Saha Institute of Nuclear Physics, 1/AF, Bidhannagar, Kolkata 700 064, India*
[5]*Department of Physics, S. V. College, Aligarh 202 001, Uttar Pradesh, India*
[6]*Department of Physics, Aligarh Muslim University, Aligarh 202 001, Uttar Pradesh, India*
[7]*Department of Physics and Astrophysics, Delhi University, Delhi 110 007, India*
[8]*Department of Physics, Gauhati University, Guwahati 781 014, Assam, India*
[9]*Nuclear Physics Division, Bhabha Atomic Research Centre, Mumbai 400 085, India*

(Received 17 October 2018; published 5 February 2019)

Background: In heavy-ion induced reactions, the sub-barrier fusion cross sections are found to be higher as compared to the predictions of the one-dimensional barrier penetration model. Attempts have been made to explain sub-barrier fusion enhancement by including the static deformations, the couplings to inelastic excitations, and non-fusion channels.

Purpose: To investigate factors which influence the sub-barrier fusion in the ^{37}Cl + ^{130}Te system and to understand the interplay of couplings, the fusion excitation function was measured at energies from 10% below to 15% above the Bass barrier.

Method: The fusion excitation function was measured by employing a recoil mass spectrometer, the Heavy-Ion Reaction Analyser (HIRA), at the Inter-University Accelerator Centre, New Delhi. To study the behavior of the fusion excitation function and the effect of couplings at sub-barrier energies, the excitation function was analyzed in the framework of the coupled-channels code CCFULL.

Results: In the present work, the fusion cross section was measured down to 1 μb at the lowest measured energy, i.e., 10% below the barrier. It was found that the inclusion of couplings of low-lying excited states along with the modified barrier between interacting nuclei satisfactorily reproduces the fusion excitation function of the ^{37}Cl + ^{130}Te system. For better insight into the sub-barrier fusion, the fusion barrier distribution, the logarithmic derivative L(E) factor, and the astrophysical S factor were extracted from the analysis of the experimentally measured fusion excitation function.

Conclusions: The analysis of the fusion excitation function in terms of the astrophysical S factor and the L(E) factor suggests the absence of fusion hindrance in the ^{37}Cl + ^{130}Te system down to a 1 μb cross section achieved at the lowest measured energy. The excitation function of the present system is compared with the existing measurements in which ^{37}Cl has been used as a projectile to understand the interplay of entrance-channel parameters in sub-barrier fusion enhancement.

DOI: 10.1103/PhysRevC.99.024607

I. INTRODUCTION

In heavy-ion induced reactions, a massive rearrangement of a complex quantum system takes place with the repetitive interactions of all nucleonic degrees of freedom between the interacting partners [1–4]. According to the simplest barrier-passing model, fusion occurs only if the energy of the incident projectile overcomes the residual barrier, formed due to equilibration of an attractive nuclear potential and the repulsive Coulomb potential between the interacting partners. However, it has been found that the nuclear interactions lead to fusion even at sub-barrier energies, i.e., $E_{c.m.} \leqslant V_b$, which has been attributed to the quantum tunneling through the barrier [5], termed the one-dimensional barrier penetration model (1D BPM). A significant enhancement in the sub-barrier fusion cross sections over the predictions of the 1D BPM has been observed [1,2]. Hence, nuclear fusion around the barrier has been extensively investigated in the past few decades to improve the understanding of the underlying dynamics [2,6–13].

The enhancement in sub-barrier fusion cross sections provides a doorway to introduce the effect of static and dynamic deformations and, subsequently, the coupling of inelastic excitations [14,15]. These couplings transform the one-dimensional single barrier into multiple barriers and,

*rnsahoo@iitrpr.ac.in
†pps@iitrpr.ac.in

consequently, reduce the strength of the original barrier, which leads to sub-barrier fusion [16–19]. Although the inclusion of couplings explained the enhancement of sub-barrier fusion cross sections over the standard 1D BPM calculations in some cases, the simultaneous interpretation of fusion cross section from sub- to above-barrier energies is found to be inconsistent, which may be an indication of coupling of non-fusing channels at below-barrier energies [20–23]. It has been observed that the presence of positive Q-value neutron transfer (PQNT) channels enhances fusion cross sections at sub-barrier energies [24–29]. However, this effect has been found to be negligible in some studies [30–35]. This suggests that the inclusion of PQNT channels may not be sufficient, but is necessary to explain an additional enhancement in sub-barrier fusion cross sections over the prediction of coupled-channels calculations [36–38].

Furthermore, Jiang *et al.* [11,39] observed that the fusion excitation function for a few systems shows an unexpected behavior with a much steeper falloff than that predicted by conventional coupled-channels calculations, termed fusion hindrance [11,40]. The phenomenon of fusion hindrance, observed initially in symmetric systems involving medium-heavy nuclei at sub-barrier energies, has been emphasized through the astrophysical S factor [41,42], and the logarithmic derivative L(E) factor [11,39,43]. The S factor and L(E) factor provide a possibility to interpret the steep falloff of fusion cross sections at deep sub-barrier energies as a signature of fusion hindrance. To explain fusion hindrance in heavy-ion reactions, several dynamical models have been proposed. The sudden model [44] takes into account nuclear incompressibility when the interacting partners overlap by including a repulsive core in the density folded potential. Ichikawa *et al.* [45,46] proposed a model based on the adiabatic picture, in which a damping factor is imposed onto the coupling strength as a function of internuclear separation to consider a gradual change from the sudden to the adiabatic case. It has been demonstrated that this damping factor originates from the reduction of quantum vibrations when the interacting partners adiabatically approach each other for fusion [46]. Diaz-Torres *et al.* [47] and Dasgupta *et al.* [21] suggested that the influence of quantum decoherence is responsible for a decrease in coupling effects. Recently, Simenel *et al.* [48,49] used the density constrained frozen Hartree-Fock method to show the reduction in tunneling probability as a result of the Pauli exclusion principle and showed that the Coulomb reorientation modifies the fusion cross section around the barrier for light deformed nuclei.

Despite the existing studies, sub-barrier fusion is not yet fully understood. This suggests that the dynamics of heavy-ion fusion is more complex than a simple inclusion of couplings of inelastic excitations between the interacting partners and non-fusion channels and thus continues to be an active area of investigation [11,21,50,51]. A rich set of fusion data is required to establish the behavior of fusion at sub-barrier energies and for the improvement of existing theoretical models. Intending to investigate different aspects of sub-barrier fusion, we measured fusion cross sections for the ^{37}Cl + ^{130}Te system at energies available at the center of mass frame ($E_{c.m.}$) from 93.68 to 120.18 MeV, i.e., from 10% below to 15% above the Coulomb barrier. The present work is a part of our efforts to understand the effect of positive Q-value neutron transfer channels on sub-barrier fusion in ^{35,37}Cl + ^{130}Te systems. The ^{35}Cl + ^{130}Te system has six positive Q-value neutron transfer channels, whereas there is none in ^{37}Cl + ^{130}Te system. This makes the ^{37}Cl + ^{130}Te system a less complex case to interpret in the framework of coupled-channels code, and thus our choice to begin with. In this work, the fusion cross-section measurement is extended down to 1 μb at the lowest measured energy. An experimentally measured excitation function was analyzed in the framework of the 1D BPM and coupled-channels formalism [20]. To understand the behavior of fusion at sub-barrier energies, the fusion barrier distribution, the L(E) factor, and the S factor were extracted from the fusion excitation function. The description of the experimental setup and data reduction methodologies (Sec. II) is followed by the presentation of the results and analysis in Sec. III. Section IV summarizes the findings of the present work.

II. EXPERIMENTAL SETUP AND METHODOLOGY

The experiment was performed at the 15UD Pelletron accelerator [52] facility of the Inter-University Accelerator Centre, New Delhi, using the recoil mass separator HIRA (Heavy Ion Reaction Analyser) [53]. The total length of HIRA is 8.6 m, i.e., the distance between the target position and the focal plane, which consists of a Q1Q2-ED1-M-MD-ED2-Q3Q4 configuration to transport the recoiling reaction products from the reaction zone to the focal plane, without losing the energy of evaporation residues (ERs), as per their m/q values. The schematic layout of HIRA is shown in Fig. 1. The angular acceptance of the spectrometer, which is adjustable, can be varied from 1 to 10 msr. In this experiment, the angular acceptance of the spectrometer was kept at 5 msr, i.e., 2.2° polar angle.

The experimental methodology of the present work is the same as that discussed in Refs. [8,27,54,55]. However, a brief account of the experimental conditions which are unique to the present work is given here. An isotopically pure ^{130}Te (enrichment 99.15%) target of ≈175 μg/cm^2 thickness was prepared on an ≈20 μg/cm^2 thick carbon backing, as tellurium is brittle in nature and becomes unstable during the irradiations. The thickness and purity of the target were measured using a Rutherford backscattering (RBS) setup. The ^{37}Cl pulsed beams of energy ranging from 121 to 155 MeV were bombarded onto the ^{130}Te target mounted inside the target chamber of HIRA maintained at ≈10^{-6} mbar pressure.

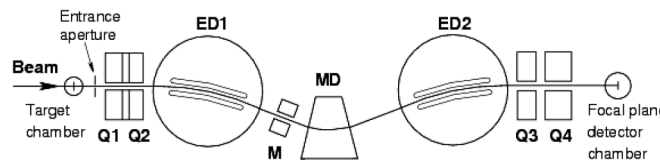

FIG. 1. A schematic layout of the recoil mass separator HIRA employed for this experiment at IUAC New Delhi.

The incident energies have been corrected for the energy loss due to target thickness by subtracting energy loss at the half thickness from its corresponding incident projectile energy. A carbon charge reset foil of thickness 30 μg/cm^2 was placed 10 cm downstream of the target for charge state equilibration of ERs reaching the focal plane of HIRA through multiple Auger processes. In the present work, the charge state distribution at different energies was not measured. The mean charge state increases with beam energy. Therefore, the charge state distribution was calculated using the Monte Carlo simulation code TERS [56] at each energy point to estimate the transmission efficiency of HIRA during the experiment, and the separator was tuned for the most probable charge state. The fraction of the most probable charge state (17^+) of the total charge state distribution at $E_{lab} = 136$ MeV is found to be 0.18 (i.e., 18%). The same can be quoted at other energy points as well. Two silicon surface barrier detectors provided with a 1-mm-diam entrance aperture were mounted inside the target chamber at a $\pm 15.5^\circ$ angle with respect to the incident beam direction to monitor the beam and to calculate the normalized cross section of ERs. Counts in the two monitor detectors were closely monitored to maintain the ratio as unity, and the same was not allowed to vary beyond 5%. Whenever more deviation was noticed, the beam was steered to keep the ratio of the counts in the two monitor detectors within the acceptable limit. Pulsed beams were used to get a clear separation between projectile-like particles and forward recoiling ERs. The time interval between two successive pulses was slightly more than the time of flight (TOF) of ERs, from the reaction point to the focal plane of HIRA. For the ^{37}Cl + ^{130}Te system, the time interval between two pulses was kept at 2 μs as the time of flight of ERs was estimated to be $\approx$1.5 μs for energy around the Bass barrier ($V_B = 104.24$ MeV).

To detect the ERs, one position-sensitive multi-wire proportional counter (MWPC) of an active area of 150 $\times$ 50 mm^2 was employed at the focal plane of HIRA. The timing information was obtained through a time-to-amplitude converter (TAC) with the arrival of particles at the focal plane as the start signal, and the delayed RF as the stop signal. The timing information was very useful for the separation of scattered beam-like particles from the ERs at the focal plane. The spectrometer was optimized for the mean charge state, mass, and energy of ERs at different incident energies. The best setting of the spectrometer was achieved by looking at the maximum transmission efficiency and clear separation of beam-like particles from ERs. The ERs were identified by making an electronic gate between timing, i.e., the actual flight time of ERs subtracted from repetition time between two pulses, and corresponding energy loss (ΔE) was measured in the MWPC. Since the group of ERs was very clearly identifiable, the timing calibration was not performed. However, the electronic delay introduced in start and/or stop signals used for generating TOF signal was left undisturbed during the experiment. Thus, the relative timing calibration was maintained between different beam energy points. This enabled us to calculate the shift in channel numbers of the mean TOF (along the y axis of Fig. 2) when beam energy was changed, which was crucial while placing the rectangular gate at the lowest energy points.

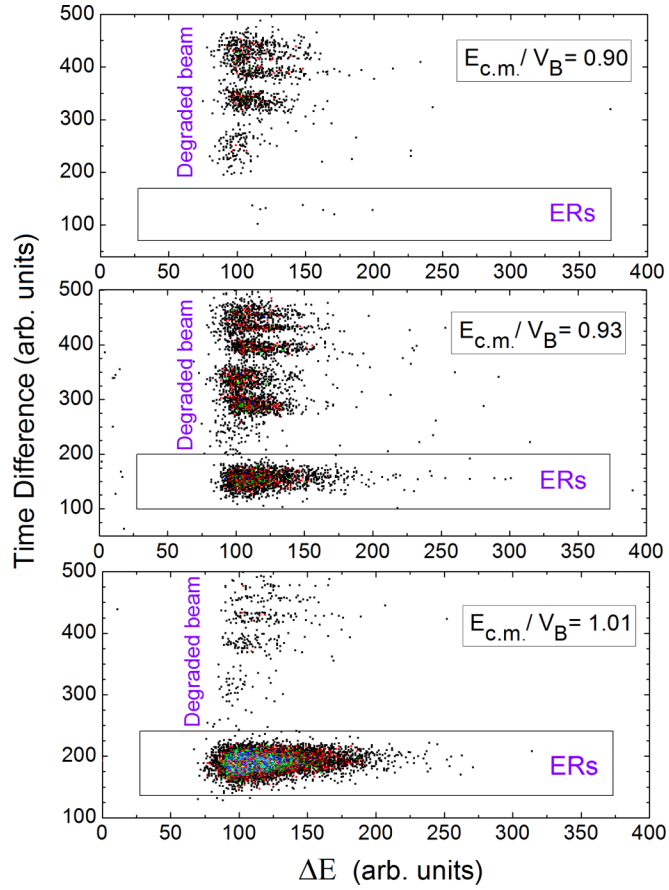

FIG. 2. Two-dimensional -time spectra obtained for the ^{37}Cl + ^{130}Te system at $E_{c.m.}/V_B = 0.90$, 0.93, and 1.01. The group of ERs and the beam-like particles are well separated from each other. The rectangles enclosing the ERs at different energies were used to account for the fusion events. Both x and y axes are displayed in arbitrary units (channel numbers).

As a representative case, ΔE-time spectra obtained for the ^{37}Cl + ^{130}Te system at $E_{c.m.}/V_B = 0.90$, 0.93, and 1.01 are presented in Fig. 2, where the ERs are clearly separated from the projectile-like particles. At the lowest measured energy, i.e., $E_{c.m.}/V_B = 0.90$, only eight ER events have been recorded in a duration of 7.5 h with beam current $\approx$2 pnA. To correct for any unwanted background and to obtain a precise cross section at this energy, a run of 2-h duration with blank target frame was taken in which no event was detected within the gate specified for ERs. Furthermore, the cross sections of ERs in the ^{37}Cl + ^{130}Te system are assumed to be fusion cross sections as the contribution of fission in this system is found to be negligible at the studied energy range [57]. The fusion cross section at different energies was estimated using the expression

$$\sigma_{fus}(E) = \frac{1}{\eta}\left(\frac{Y_{ER}}{Y_M}\right)\left(\frac{d\sigma}{d\Omega}\right)_R \Omega_M, \quad (1)$$

where η is the average ER transmission efficiency of HIRA, Y_{ER} is the yield of evaporation ERs at the focal plane, $Y_M = (M_L M_R)^{1/2}$ is the geometric mean of monitor yields, $(\frac{d\sigma}{d\Omega})_R$ is the Rutherford differential cross section, and Ω_M is the solid angle subtended by the monitor detectors with respect to the beam direction.

The transmission efficiency of HIRA (η) is defined as the ratio of ERs reaching the focal plane to the ERs produced at the target. Experimentally, the transmission efficiency of HIRA is extracted using the particle-gamma coincidence [27]. For the present system, the transmission efficiency of HIRA is calculated using the semi-microscopic Monte Carlo code TERS [56], which has been found to reproduce the efficiency of HIRA within an accuracy of 10% [8,55]. The value of monitor yield, Y_M, is the geometric mean of monitor counts M_L and M_R. The Rutherford scattering cross sections are calculated at different energies by using the following expression:

$$\left\{\frac{d\sigma}{d\Omega}\right\}_R^L = \left\{\frac{1.138 Z_P Z_T}{E_L}\right\}^2 \left\{\frac{1}{\sin^4(\theta_L/2)} - 2\left[\frac{M_P}{M_T}\right]^2\right\}, \quad (2)$$

where Z_P, M_P, Z_T, and M_T represent the respective charge and mass of the projectile and the target nuclei, and E_L and θ_L are the bombarding energy and scattering angle in the laboratory frame, respectively.

III. RESULTS AND INTERPRETATIONS

The excitation function for the $^{37}Cl + ^{130}Te$ system was generated by measuring fusion cross sections from 10% below the barrier to 15% above the barrier and is represented in Fig. 3. The experimentally measured fusion cross sections and corresponding error are given in Table I. The presented errors are absolute errors consisting of the statistical error and error in the transmission efficiency of HIRA. As can be seen in Fig. 3, the fusion cross section was measured down to 1 μb at the lowest measured energy in the present work.

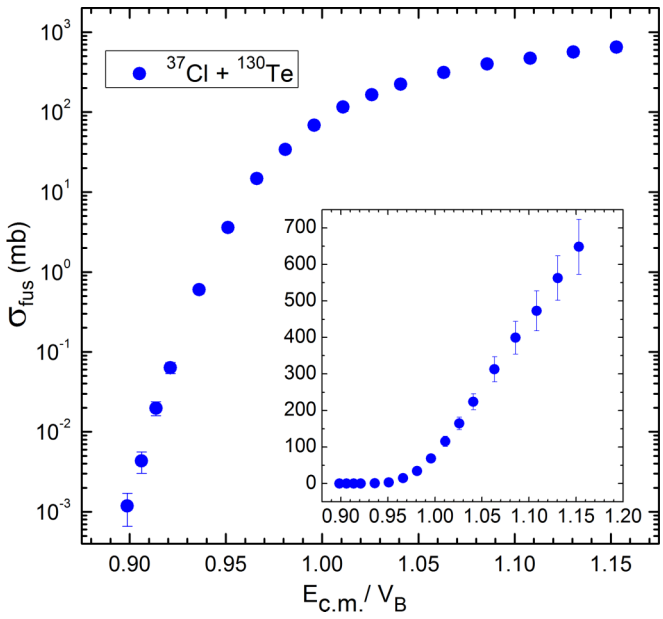

FIG. 3. Experimentally measured fusion excitation function for the $^{37}Cl + ^{130}Te$ system. The inset shows fusion cross sections in linear scale for better visualization of fusion excitation functions in above-barrier energies. Uncertainty in a few data points is hidden in the size of the symbol.

TABLE I. Experimentally measured fusion cross sections (σ_{fus}) for the $^{37}Cl + ^{130}Te$ system from $E_{c.m.} = 93.68$ to 120.18 MeV, i.e., from 10% sub- to 15% above- barrier energies.

$E_{c.m.}$ (MeV)	$\sigma_{fus} \pm \delta\sigma_{fus}$ (mb)	$E_{c.m.}$ (MeV)	$\sigma_{fus} \pm \delta\sigma_{fus}$ (mb)
93.68	0.0012 ± 0.0005	105.37	115 ± 14
94.46	0.0043 ± 0.0001	106.93	165 ± 17
95.24	0.012 ± 0.004	108.49	224 ± 22
96.02	0.063 ± 0.011	110.83	313 ± 34
97.58	0.602 ± 0.075	113.17	399 ± 45
99.14	3.59 ± 0.38	115.51	473 ± 55
100.70	14.71 ± 1.65	117.85	562 ± 63
102.25	34 ± 4	120.18	648 ± 75
103.81	68 ± 8		

A. Analysis with CCFULL code

The coupled-channels code CCFULL has been used to interpret the trend of fusion cross sections at sub-barrier energies and to put the fusion data in a perspective that can be a convenient starting point for further theoretical treatment [20]. This code has the scope to calculate fusion cross sections with or without considering inelastic excitations of interacting partners. The predictions of cross sections without implementing inelastic excitations are considered in the 1D BPM. It is formulated by taking the distance of closest approach and the interacting potential between the interacting nuclei, and the σ_{fus} can be expressed as

$$\sigma_{fus} = \frac{\hbar\omega R_b^2}{2E_{c.m.}} \ln\left\{1 + \exp\left[\frac{2\pi}{\hbar\omega}(E_{c.m.} - V_B)\right]\right\}, \quad (3)$$

where $\hbar\omega$, R_b, $E_{c.m.}$, and V_B represent the barrier curvature, barrier radius, available energy in the center-of-mass frame, and residual barrier, respectively.

Recently, various types of potential have been proposed to explain fusion data over different energy ranges. The ion-ion potential used in the present work is the Akyuz-Winther (AW) potential where the parameters are $V_0 = 74$ MeV, $r_0 = 1.18$ fm, and $a_0 = 0.67$ fm [58–61]. The most sensitive and critical parameter of the nuclear potential is the diffuseness (a_0), which affects the slope of the nuclear potential in the surface region, and thus the curvature of the effective potential. The magnitude of diffuseness changes with bombarding energy, due to the strong influence of density distributions inside the composite system.

To understand the effect of diffuseness on fusion, an experimentally measured excitation function for the $^{37}Cl + ^{130}Te$ system is compared with the prediction of the 1D BPM by changing the numerical value of the diffuseness parameter from 0.67 to 0.90 fm in Fig. 4. As can be seen in this figure, the standard AW treatment, with diffuseness parameter 0.67 fm, does not reproduce the fusion excitation function for

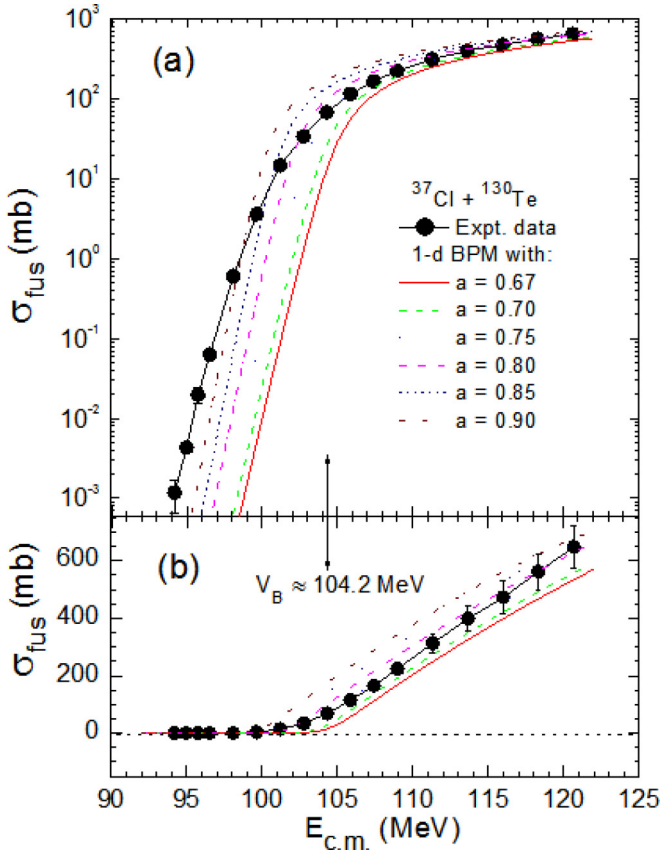

FIG. 4. The fusion excitation function for the ^{37}Cl + ^{130}Te system is compared with that calculated using the 1D BPM for different values of diffuseness parameter, ranging from 0.67 to 0.90 fm, as discussed in the text. Total errors, statistical plus systematic ones, are included. Lines and curves are self-explanatory.

the entire measured energy range. The calculations performed using higher values of diffuseness parameter predict larger fusion cross sections at sub- and above-barrier energies, but do not reproduce the fusion excitation function at around the barrier for the presently studied system. This discrepancy indicates the unknown nature of the nuclear potential and/or the involvement of other non-fusing reaction channels [58]. On the basis of the results presented in Fig. 4, it may be inferred that the incident energy influences the diffuseness and subsequently the nuclear potential. The energy-dependent nuclear potential brings different dynamical factors with various incident energy regimes. As such, the inclusion of couplings of inelastic excitations and non-fusion channels may be used to explain the fusion excitation function.

Figure 5 shows the coupled-channels calculations for different inelastic excitations of the interacting partners. The calculations were performed using a Woods-Saxon form of the AW potential. The spectroscopic properties of the interacting partners, ^{37}Cl and ^{130}Te, used in the coupled-channels calculations are given in Table II [20,62,63]. As CCFULL can include all orders of couplings, the experimentally measured fusion excitation function was compared with the coupled-channels calculations by imposing different excited states of interacting partners without changing the potential parameters.

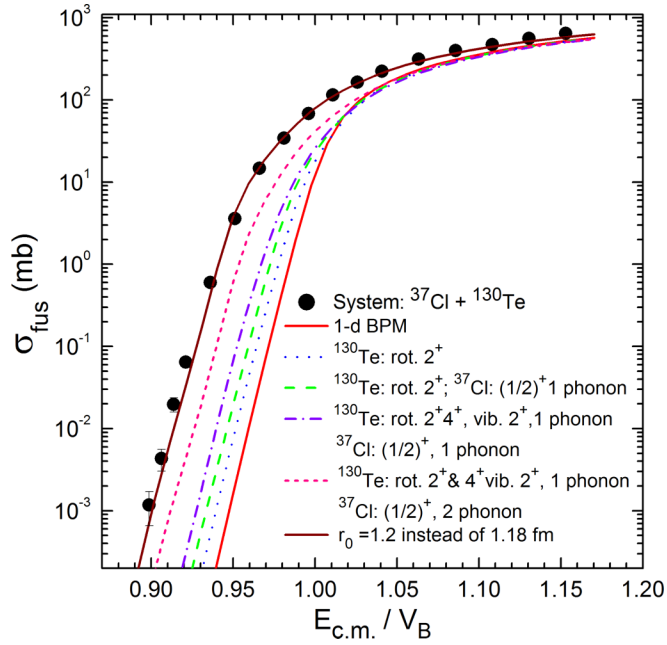

FIG. 5. The experimentally measured excitation function is compared with the 1D BPM and for different modes of coupling between interacting partners using CCFULL. It shows that the inclusion of couplings of different inelastic excitations of interacting partners with radius parameter $r_0 = 1.2$ fm reproduces the experimental excitation function fairly well. Lines and curves are self-explanatory.

As shown in Fig. 5, by the inclusion of the 2^+ rotational state of the ^{130}Te target and ^{37}Cl projectile as inert, the coupled-channels calculation under-predicts the experimental excitation function but enhances the fusion cross section as compared to 1D BPM calculations. When the rotational 2^+ state of ^{130}Te and $\frac{1}{2}^+$ vibrational state of the ^{37}Cl projectile with one-phonon coupling were taken into account, the sub-barrier fusion cross sections were enhanced significantly as compared to the previous values. Similarly, other coupling conditions were included in the CCFULL calculations as presented in Fig. 5. It may be pointed out that the inclusion of 2^+ and 4^+ states as well as the 2^+ vibrational state with one-phonon coupling of the ^{130}Te target, and the $\frac{1}{2}^+$ state of the ^{37}Cl projectile with two-phonon coupling, further enhances the sub-barrier fusion cross sections but fails to reproduce the experimentally measured fusion excitation function. However, the interaction potential is slightly modified by changing the

TABLE II. Deformation parameters and excitation energies along with the spectroscopic properties of ^{37}Cl and ^{130}Te nuclei used in the coupled-channels calculations [20,62,63].

Nucleus	E_{ex} (MeV)	I^π	$E(\lambda)$	β
^{37}Cl	1.73	vib. $(1/2)^+$	2	0.14
	3.09	vib. $(5/2)^+$	2	0.24
^{130}Te	0.83	rot. 2^+	2	0.11
	2.45	rot. 4^+	2	0.11
	1.59	vib. 2^+	2	0.11

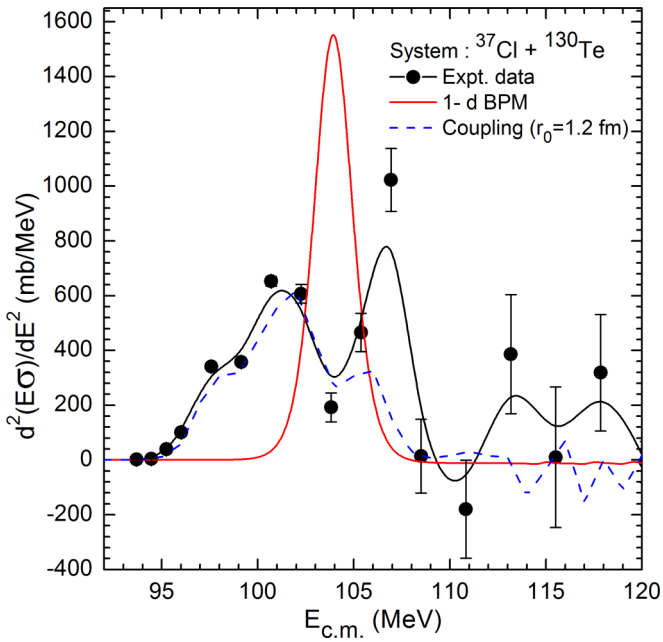

FIG. 6. The fusion barrier distribution for the ^{37}Cl + ^{130}Te system. The experimental fusion distribution is broad and splits into multiple components, while the prediction of the 1D BPM shows a single peak at the undivided barrier energy. Lines and curves are self-explanatory.

radius parameter to $r_0 = 1.2$ fm instead of $r_0 = 1.18$ fm in the coupled-channels calculations with the same set of target and projectile excitations [64]. It can be seen in Fig. 5 that the experimental fusion excitation function is well reproduced within the experimental uncertainties. On the basis of the analysis presented here, it may be inferred that a slight change in potential parameters is required to interpret fusion at sub-barrier energies along with the inclusion of couplings in the coupled-channels approach.

B. Fusion barrier distribution

In heavy-ion reactions, fusion at sub-barrier energies has been interpreted by including couplings of low-lying excited states owning to inelastic excitations, and transfer channels [14,18–21,23–25]. It has been found that the couplings of inelastic excited states modify the single barrier into multiple components by reducing its original strength, leading to the sub-barrier fusion. Therefore, the fusion barrier distribution may be used as a fingerprint to probe the nature of couplings involved in sub-barrier fusion [16,17,64,65]. The fusion barrier distribution is expressed as the second energy derivative of the fusion cross section times the energy, that is,

$$D_{fus}(E) = \frac{d^2(E\sigma_{fus})}{dE^2}, \tag{4}$$

where σ_{fus} represents the fusion cross section, and E is its corresponding beam energy.

Figure 6 shows the fusion barrier distribution obtained by double differentiation of the fusion excitation function for the ^{37}Cl + ^{130}Te system. As can be seen in this figure, the experimental fusion barrier distribution is found to be broad and splits into two peaks around the barrier. This may be due to the coupling of low-lying excited states resulting from the inelastic excitations of interacting partners as described in connection with Fig. 5. Therefore, it may be inferred that the higher-order couplings due to nuclear-surface vibrations and collective rotation play an important role in sub-barrier fusion. Furthermore, as shown in Fig. 6, the shape of the experimental barrier distribution closely resembles the predictions of the coupled-channels calculations in the first part, i.e., below $E_{c.m.} \approx 105$ MeV. However, in the second part, the height of the experimental barrier is found to be more as compared to the coupled-channels calculations, which signifies the involvement of non-fusion channels and/or that the couplings do not influence the above-barrier fusion. The involvement of inelastic couplings well reproduces the measured sub-barrier fusion cross sections for the systems with no positive Q-value neutron transfer channels. To probe the behavior of the measured fusion excitation function at extremely below-barrier energies the astrophysical S factor and the logarithmic derivative L(E) factor are derived and compared with that predicted by CCFULL.

C. Astrophysical S factor

The astrophysical S factor is a useful procedure to interpret fusion cross sections at zero center-of-mass energy using the extrapolation of the experimentally measured fusion excitation function [41,66]. The S factor is defined in terms of the fusion cross section, $\sigma_{fus}(E)$, as

$$S(E) = \frac{E_{cm}\sigma_{fus}(E)}{\exp(-2\pi\eta)}, \tag{5}$$

where E_{cm} is the center-of-mass energy, $\sigma_{fus}(E)$ is the fusion cross section, and η is the Sommerfeld parameter. The Sommerfeld parameter can be expressed as

$$\eta = \frac{Z_1 Z_2 e^2}{\hbar v} \quad \text{or} \quad \alpha Z_1 Z_2 \sqrt{\frac{\mu c^2}{2E_{c.m.}}},$$

where v is the beam velocity, μ is the reduced mass of the system, and Z_1 and Z_2 are the charges of projectile and target nuclei, respectively.

The Gamow factor $(-2\pi\eta)$ in the denominator of the S-factor expression accounts for the main part of the strong energy dependence of the fusion cross sections in light-ion induced fusion reactions such that the S factor is essentially a constant or display a very weak dependence at deep sub-barrier energies. It may be pointed out that the fusion in positive Q-value systems can take place even at zero center-of-mass energy, and the S factor is often extrapolated to $E = 0$. However, for the medium-heavy systems with $Z_1Z_2[A_1A_2/(A_1 + A_2)]^{1/2} > 1500$, where the ground state Q values are negative, the S-factor interpretation is needed. In heavy-ion induced reactions, the fusion cross sections drop rapidly with decrease in bombarding energy, corresponding to an energy point where the fusion is forbidden. The S factor must reach a maximum at a particular energy and below which the fusion cross sections drop significantly, which is considered a signature of the fusion hindrance [42,67]. To

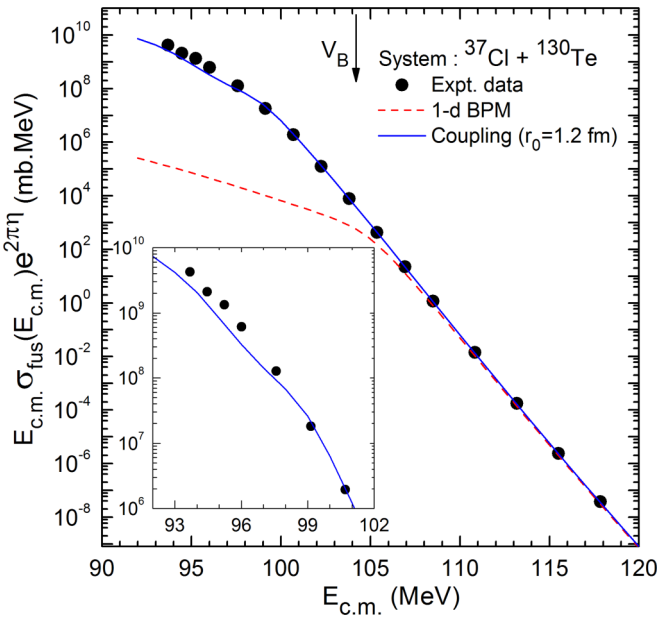

FIG. 7. Astrophysical S factor derived from experimental fusion cross sections in the ^{37}Cl + ^{130}Te system. The lines and curves are self-explanatory. The top portion of this figure is magnified in the inset to show discrepancy in experimental data with coupled-channel calculations.

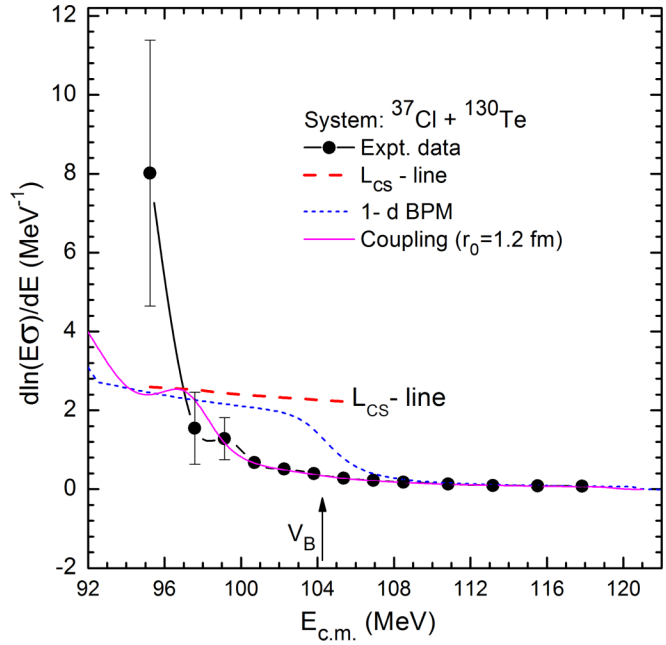

FIG. 8. The logarithmic derivative L(E) factor plotted as a function of the center-of-mass energy for the ^{37}Cl + ^{130}Te system. Lines and curves are self-explanatory.

probe if the astrophysical S factor reaches a maximum for the ^{37}Cl + ^{130}Te system, the experimental fusion excitation function was analyzed to extract the astrophysical S factor and compared with the prediction of the 1D BPM and coupled-channels approach in Fig. 7.

As can be seen from this figure, the astrophysical S factor does not show a maximum and exhibits a continuous increase for the entire sub-barrier energy range. The absence of an S-factor maximum signifies the absence of fusion hindrance for the ^{37}Cl + ^{130}Te system in the measured energy range which is due to multiple barriers, caused by the static and dynamic deformations, which leads to different turning points depending on the mutual orientation and excitation of interacting nuclei. The S factor predicted by the 1D BPM appears to be saturated just below the barrier but the experimentally extracted S factor increases steeply and is found to be in good agreement with the coupled-channels calculations as shown in Fig. 7. Moreover, the inset of Fig. 7 shows that the coupled-channels calculations slightly under-predict a few experimental data points, below $E_{c.m.} = 96$ MeV. This may be an indication of the evolution of other reaction channels at deep sub-barrier energies.

D. L(E) factor

The trend of fusion cross sections was studied in the S-factor illustration at the lowest energies where no maximum has been seen in this work, indicating no fusion hindrance down to 1 μb cross section at the lowest measured energy. For some systems, where it is not necessary to achieve an S-factor maximum, the fusion hindrance in the rapidly changing sub-barrier fusion cross sections may be recognized by an alternative pragmatic representation, the logarithmic derivative L(E) factor [11,39,43]. This is defined as the energy-weighted fusion cross sections,

$$L(E) = \frac{d[ln(E\sigma)]}{dE} = \frac{1}{E\sigma}\frac{d(E\sigma)}{dE}, \quad (6)$$

and shows a strong increase around the energy point where the S factor reaches its maximum. It may be pointed out that when the S factor reaches its maximum, the L(E)-factor curve gets saturated. The advantage of the S factor is that it gives a simple and direct representation of the fusion excitation function, whereas the logarithmic derivative and the barrier distribution are more indirectly derived quantities. At deep sub-barrier energies, the L(E) factor is proven to be a conclusive tool for the excitation function analysis.

To study the behavior of the fusion cross section σ_{fus} with decreasing energy in the sub-barrier region, the L(E) factor was extracted for the ^{37}Cl + ^{130}Te system by using the central difference method of differentiation by keeping the same interval between the data points, as shown in Fig. 8. In this figure, the experimental L(E) factor is compared with that predicted by the 1D BPM and coupled-channels approach by including suitable couplings as shown in Fig 5. As can be seen in Fig. 8, the experimental L(E) factor keeps rising towards the lowest measured energy, which suggests the absence of fusion hindrance even though the present measurement has been extended down to a 1 μb cross section. According to Jiang *et al.* [10,11,51,67], the soft systems do not exhibit fusion hindrance until 7–15 MeV lower than the systematics for stiff systems with negative Q value. The present system does not show any exception to the systematics and can be considered a soft system.

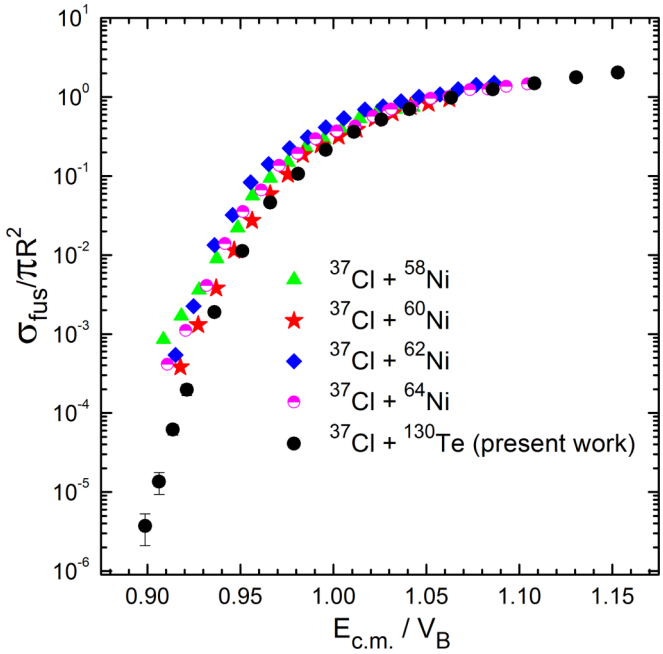

FIG. 9. Reduced fusion excitation functions of ^{37}Cl as a projectile on different targets are compared with the presently studied system, ^{37}Cl + ^{130}Te. Fusion cross sections for comparison are from Ref. [68].

E. Comparison of ^{37}Cl + ^{58,60,62,64}Ni, ^{130}Te systems

To generate some systematics for fusion at sub-barrier energies, the excitation functions for ^{37}Cl + ^{58,60,62,64}Ni, ^{130}Te systems are compared in Fig. 9. As shown in this figure, the fusion cross sections (σ_{fus}) are normalized with a geometrical cross section (πR^2), and the bombarding energies ($E_{c.m.}$) are normalized with Bass barrier height (V_B) to incorporate the effects of nuclear radius and barriers of different systems in comparison [30]. The radius is calculated as $R = r_0(A_P^{1/3} + A_T^{1/3})$, where r_0=1.2 fm, and A_P and A_T represent the mass of the projectile and target nucleus, respectively.

As can be seen in Fig. 9, the fusion cross sections for ^{37}Cl + ^{130}Te system (present work) are somewhat lower than that of ^{37}Cl + ^{58,60,62,64}Ni systems [68]. It may be pointed out that the fusion cross section in the present work is achieved down to 1 μb which is two orders of magnitude less than that measured for ^{37}Cl+Ni systems. The spectroscopic properties of reactions in comparison, e.g., deformation, N/Z ratio, fusion Q value (Q_{fus}), and the ground state Q value (Q_{gg}) of neutron pick-up channels, are presented in Tables III and IV for all systems compared in Fig. 9.

As shown in Table III, the deformation parameter of ^{130}Te is nearly half as compared to Ni isotopes; thus, the one-dimensional barrier height of the ^{37}Cl + ^{130}Te system comparatively decreased, hence the fusion probability. The fusion Q value of the ^{37}Cl + ^{130}Te system is 4.5 times smaller as compared to ^{37}Cl + ^{58,60,62,64}Ni systems. The more negative fusion Q value restricts the interacting partners to be fused, suggesting less fusion probability in the case of the present system. The excitation energies of low-lying excited states (E_{ex}) of ^{37}Cl and Ni isotopes are almost the same. The value of E^* for ^{130}Te is significantly less than the Ni isotopes. Since the excitation energies are similar in the case of ^{37}Cl and Ni isotopes, this may lead to more favorable couplings as compared to ^{130}Te nuclei, and therefore the enhanced fusion cross sections for Ni isotopes as compared to the ^{130}Te. Furthermore, as shown in Table IV, the ground state Q values of all neutron transfer channels are negative for ^{37}Cl + ^{58,60,62,64}Ni, ^{130}Te systems. As such, it may be concluded that the transfer channels are not suitable to explain these excitation functions.

TABLE III. Excitation energies (E^*), angular momentum and parity (I^π), transition E(λ), deformation parameter (β), and N/Z value of targets selected for comparison [62,63,68]. Fusion Q values (Q_{fus}) of different targets with ^{37}Cl projectile are presented in this table.

Nucleus	E^* (MeV)	I^π	E(λ)	β	N/Z	Q_{fus} (MeV)
^{58}Ni	1.45	2^+	2	0.20	1.07	−13.65
	4.47	3^-	3	0.21		
^{60}Ni	1.33	2^+	2	0.22	1.14	−13.68
	4.04	3^-	3	0.19		
^{62}Ni	1.17	2^+	2	0.21	1.21	−12.93
	3.75	3^-	3	0.22		
^{64}Ni	1.35	2^+	2	0.19	1.28	−11.45
	3.58	3^-	3	0.22		
^{130}Te	0.83	2^+	2	0.11	1.50	−56.57
	1.59	2^+	2	0.11		

IV. SUMMARY AND CONCLUSIONS

In the present work, the fusion excitation function of the ^{37}Cl + ^{130}Te system was measured from $E_{c.m.}$ ≈ 94 to ≈120 MeV, i.e., from 10% below to 15% above the Bass barrier. To study the behavior of fusion in the sub-barrier energy region, the measurement of fusion cross sections was extended down to 1 μb at the lowest measured energy. The experimentally measured fusion excitation function was analyzed in the framework of the coupled-channels code CCFULL. The fusion excitation function is found to be significantly higher than the predictions of the 1D BPM, where the standard Akyuz-Winther potential parameters were used. The sub-barrier fusion enhancement was explained by the inclusion of inelastic couplings and modified potential. In order to

TABLE IV. The ground state Q value (Q_{gg}) of neutron pick-up channels in MeV from 1n to 6n transfer channels for different projectile-target combinations used for comparison in Fig. 9.

System	1n	2n	3n	4n	5n	6n
^{37}Cl + ^{58}Ni	−6.11	−8.23	−19.1	−25.4	−37.44	−44.2
^{37}Cl + ^{60}Ni	−5.28	−6.20	−12.6	−15.02	−25.9	−32.7
^{37}Cl + ^{62}Ni	−4.49	−4.23	−9.80	−10.1	−17.5	−20.2
^{37}Cl + ^{64}Ni	−3.54	−2.31	−7.08	−7.08	−12.8	−14.3
^{37}Cl + ^{130}Te	−2.31	−0.32	−3.27	−1.74	−5.18	−4.26

interpret the trend of rapidly changing fusion cross sections at sub-barrier energies, the experimentally measured fusion excitation function was processed to extract the fusion barrier distribution, the astrophysical S factor, and the L(E) factor. It was observed that the original one-dimensional barrier splits into multiple components with a complex structure around the barrier owing to couplings of low-lying excited states of interacting partners. The astrophysical S factor does not attain a maximum, and no saturation was observed in the L(E)-factor curve for the ^{37}Cl + ^{130}Te system even for the fusion cross section as low as 1 μb measured at an energy ≈10% below the barrier. The results and analysis presented in this work suggest the absence of fusion hindrance for the ^{37}Cl + ^{130}Te system down to 10% below the barrier. The fusion excitation function achieved in this work was compared with a few systems where the same projectile (^{37}Cl) was used. The comparative analysis indicates that the sub-barrier fusion is sensitive to the deformation and consequently to the inelastic excitations and ground state fusion Q value of the reaction.

ACKNOWLEDGMENTS

The authors acknowledge the IUAC Pelletron crew for providing ^{37}Cl beams of requisite quality and the IUAC target laboratory for the help during target fabrication. One of the authors, R.N.S., thanks Prof. H. J. Wollersheim, Prof. R. G. Pillay, and Prof. S. Kailas for their critical suggestions, and P.P.S. acknowledges a startup grant from the Indian Institute of Technology Ropar, the Council of Scientific and Industrial Research for Research Grant No. CSIR/03(1353)/16/EMR-II, and the Science and Engineering Research Board for Young Scientist Award No. YSS/2014/000250.

[1] B. B. Back, H. Esbensen, C. L. Jiang, and K. E. Rehm, Rev. Mod. Phys. **86**, 317 (2014), and references therein.
[2] M. Dasgupta, D. J. Hinde, N. Rowlay, and A. M. Stefanini, Annu. Rev. Nucl. Part. Sci. **48**, 401 (1998).
[3] A. B. Balantekin and N. Takigawa, Rev. Mod. Phys. **70**, 77 (1998).
[4] C. Y. Wu, W. V. Oertzen, D. Cline, and M. W. Guidy, Annu. Rev. Nucl. Part. Sci. **40**, 285 (1990).
[5] C. Y. Wong, Phys. Lett. B **42**, 186 (1972); Phys. Rev. Lett. **31**, 766 (1973).
[6] G. Colucci, G. Montagnoli, A. M. Stefanini, H. Esbensen, D. Bourgin, P. Čolović, L. Corradi, M. Faggian, E. Fioretto, F. Galtarossa, A. Goasduff, J. Grebosz, F. Haas, M. Mazzocco, F. Scarlassara, C. Stefanini, E. Strano, S. Szilner, M. Urbani, and G. L. Zhang, Phys. Rev. C **97**, 044613 (2018).
[7] Md. M. Shaikh, S. Nath, J. Gehlot, T. Banerjee, I. Mukul, R. Dubey, A. Shamlath, P. V. Laveen, M. Shareef, A. Jhingan, N. Madhavan, T. Rajbongshi, P. Jisha, G. N. Jyothi, A. Tejaswi, R. N. Sahoo, and A. Rani, J. Phys. G: Nucl. Part. Phys. **45**, 095103 (2018).
[8] Khushboo, S. Mandal, S. Nath, N. Madhavan, J. Gehlot, A. Jhingan, Neeraj Kumar, T. Banerjee, G. Kaur, K. Rojeeta Devi, A. Banerjee, Neelam, T. Varughese, D. Siwal, R. Garg, Ish Mukul, M. Saxena, S. Verma, S. Kumar, B. R. Behera, P. Verma *et al.*, Phys. Rev. C **96**, 014614 (2017).
[9] L. F. Canto, P. R. S. Gomes, J. Lubian, L. C. Chamon, and E. Crema, J. Phys. G **36**, 015109 (2009).
[10] C. L. Jiang, K. E. Rehm, B. B. Back, and R. V. F. Janssens, Phys. Rev. C **75**, 015803 (2007).
[11] C. L. Jiang *et al.*, Phys. Rev. Lett. **89**, 052701 (2002); Phys. Rev. C **71**, 044613 (2005); Phys. Lett. B **640**, 18 (2006); Phys. Rev. Lett. **113**, 022701 (2014).
[12] M. Beckerman, M. Salomaa, A. Sperduto, H. Enge, J. Ball, A. DiRienzo, S. Gazes, Y. Chen, J. D. Molitoris, and Mao Naifeng, Phys. Rev. Lett. **45**, 1472 (1980).
[13] R. A. Broglia, C. H. Dasso, S. Landowne, and A. Winther, Phys. Rev. C **27**, 2433(R) (1983).
[14] R. G. Stokstad and E. E. Gross, Phys. Rev. C **23**, 281 (1981).
[15] R. G. Stokstad, Y. Eisen, S. Kaplanis, D. Pelte, U. Smilansky, and I. Tserruya, Phys. Rev. Lett. **41**, 465 (1978); Phys. Rev. C **21**, 2427 (1980).
[16] N. Rowlay, G. R. Satchler, and P. H. Stelson, Phys. Lett. B **254**, 25 (1991).
[17] O. A. Capurro, J. E. Testoni, D. Abriola, D. E. DiGregorio, J. O. Fernández Niello, G. V. Martí, A. J. Pacheco, M. R. Spinella, M. Ramírez, C. Balpardo, and M. Ortega, Phys. Rev. C **65**, 064617 (2002).
[18] A. M. Stefanini, L. Corradi, A. M. Vinodkumar, Yang Feng, F. Scarlassara, G. Montagnoli, S. Beghini, and M. Bisogno, Phys. Rev. C **62**, 014601 (2000); **65**, 034609 (2002).
[19] A. M. Stefanini, F. Scarlassara, S. Beghini, G. Montagnoli, R. Silvestri, M. Trotta, B. R. Behera, L. Corradi, E. Fioretto, A. Gadea, Y. W. Wu, S. Szilner, H. Q. Zhang, Z. H. Liu, M. Ruan, F. Yang, and N. Rowley, Phys. Rev. C **73**, 034606 (2006).
[20] K. Hagino, N. Rowley, and T. Kruppa, Comput. Phys. Commun. **123**, 143 (1999).
[21] M. Dasgupta, D. J. Hinde, A. Diaz-Torres, B. Bouriquet, Catherine I. Low, G. J. Milburn, and J. O. Newton, Phys. Rev. Lett. **99**, 192701 (2007).
[22] V. V. Sargsyan, G. G. Adamian, N. V. Antonenko, W. Scheid, and H. Q. Zhang, Phys. Rev. C **85**, 024616 (2012); **85**, 069903(E) (2012).
[23] V. V. Sargsyan, G. G. Adamian, N. V. Antonenko, W. Scheid, and H. Q. Zhang, Phys. Rev. C **91**, 014613 (2015).
[24] P. H. Stelson, H. J. Kim, M. Beckerman, D. Shapira, and R. L. Robinson, Phys. Rev. C **41**, 1584 (1990).
[25] M. Trotta, A. M. Stefanini, L. Corradi, A. Gadea, F. Scarlassara, S. Beghini, and G. Montagnoli, Phys. Rev. C **65**, 011601(R) (2001).
[26] J. J. Kolata, A. Roberts, A. M. Howard, D. Shapira, J. F. Liang, C. J. Gross, R. L. Varner, Z. Kohley, A. N. Villano, H. Amro, W. Loveland, and E. Chavez, Phys. Rev. C **85**, 054603 (2012).
[27] Sunil Kalkal, S. Mandal, N. Madhavan, E. Prasad, Shashi Verma, A. Jhingan, Rohit Sandal, S. Nath, J. Gehlot, B. R. Behera, Mansi Saxena, Savi Goyal, Davinder Siwal, Ritika Garg, U. D. Pramanik, Suresh Kumar, T. Varughese, K. S. Golda, S. Muralithar, A. K. Sinha, and R. Singh, Phys. Rev. C **81**, 044601 (2010).
[28] H. Timmers, D. Ackermann, S. Beghini, L. Corradi, J. H. He, Montagnoli, E. Scarlassara, A. M. Stefanini, and N. Rowley, Nucl. Phys. A **633**, 421 (1998).

[29] H. M. Jia, C. J. Lin, F. Yang, X. X. Xu, H. Q. Zhang, Z. H. Liu, Z. D. Wu, L. Yang, N. R. Ma, P. F. Bao, and L. J. Sun, Phys. Rev. C **89**, 064605 (2014).
[30] Z. Kohley, J. F. Liang, D. Shapira, R. L. Varner, C. J. Gross, J. M. Allmond, A. L. Caraley, E. A. Coello, F. Favela, K. Lagergren, and P. E. Mueller, Phys. Rev. Lett. **107**, 202701 (2011).
[31] A. M. Stefanini, G. Montagnoli, F. Scarlassara, C. L. Jiang, H. Esbensen, E. Fioretto, L. Corradi, B. B. Back, C. M. Deibel, B. Di Giovine, J. P. Greene, H. D. Henderson, S. T. Marley, M. Notani, N. Patel, K. E. Rehm, D. Sewerinyak, X. D. Tang, C. Ugalde, and S. Zhu, Eur. Phys. J. A **49**, 63 (2013).
[32] K. T. Lesko, W. Henning, K. E. Rehm, G. Rosner, J. P. Schiffer, G. S. F. Stephans, B. Zeidman, and W. S. Freeman, Phys. Rev. C **34**, 2155 (1986).
[33] C. J. Lin, H. M. Jia, H. Q. Zhang, X. X. Xu, F. Yang, L. Yang, P. F. Bao, L. J. Sun, and Z. H. Liu, EPJ Web Conf. **66**, 03055 (2014).
[34] M. Benjellom, W. Galster, and J. Vervier, Nucl. Phys. A **560**, 715 (1993).
[35] P. Jacobs, Z. Fraenkel, G. Mamane and I. Tserruya, Phys. Lett. B **175**, 271 (1986).
[36] V. A. Rachkov, A. V. Karpov, A. S. Denikin, and V. I. Zagrebaev, Phys. Rev. C **90**, 014614 (2014).
[37] G. L. Zhang, X. X. Liu, and C. J. Lin, Phys. Rev. C **89**, 054602 (2014).
[38] J. F. Liang, D. Shapira, C. J. Gross, J. R. Beene, J. D. Bierman, A. Galindo-Uribarri, J. G. del Campo, P. A. Hausladen, Y. Larochelle, W. Loveland, P. E. Mueller, D. Peterson, D. C. Radfrod, D. W. Stracener, and R. L. Varner, Phys. Rev. Lett. **91**, 152701 (2003); **96**, 029903 (2006).
[39] C. L. Jiang, H. Esbensen, B. B. Back, R. V. F. Janssens, and K. E. Rehm, Phys. Rev. C **69**, 014604 (2004).
[40] M. Beckerman, J. Ball, H. Enge, M. Salomaa, A. Sperduto, S. Gazes, A. DiRienzo, and J. D. Molitoris, Phys. Rev. C **23**, 1581 (1981).
[41] S. Schramm *et al.*, Astrophys. J. **365**, 296 (1990).
[42] V. V. Sargsyan, G. G. Adamian, N. V. Antonenko, W. Scheid, and H. Q. Zhang, Phys. Rev. C **95**, 054619 (2017).
[43] A. M. Stefanini, G. Montagnoli, L. Corradi, S. Courtin, D. Bourgin, E. Fioretto, A. Goasduff, J. Grebosz, F. Haas, M. Mazzocco, T. Mijatović, D. Montanari, M. Pagliaroli, C. Parascandolo, F. Scarlassara, E. Strano, S. Szilner, N. Toniolo, and D. Torresi, Phys. Rev. C **92**, 064607 (2015); R. J. Charity, *ibid.* **82**, 014610 (2010).
[44] S. Misicu and H. Esbensen, Phys. Rev. Lett. **96**, 112701 (2006); Phys. Rev. C **75**, 034606 (2007).
[45] T. Ichikawa, K. Hagino, and A. Iwamoto, Phys. Rev. Lett. **103**, 202701 (2009); Prog. Theor. Phys. Suppl. **196**, 269 (2012).
[46] T. Ichikawa, Phys. Rev. C **92**, 064604 (2015).
[47] A. Diaz-Torres, D. J. Hinde, M. Dasgupta, G. J. Milburn, and J. A. Tostevin, Phys. Rev. C **78**, 064604 (2008); A. Diaz-Torres, *ibid.* **81**, 041603(R) (2010).
[48] C. Simenel, A. S. Umar, K. Godbey, M. Dasgupta, and D. J. Hinde, Phys. Rev. C **95**, 031601(R) (2017).
[49] C. Simenel, Ph. Chomaz, and G. de France, Phys. Rev. Lett. **93**, 102701 (2004).
[50] A. M. Stefanini, G. Montagnoli, R. Silvestri, L. Corradi, S. Courtin, E. Fioretto, B. Guiot, F. Haas, D. Lebhertz, P. Mason, F. Scarlassara, and S. Szilner, Phys. Lett. B **679**, 95 (2009).
[51] C. L. Jiang, B. B. Back, H. Esbensen, R. V. F. Janssens, and K. E. Rehm, Phys. Rev. C **73**, 014613 (2006).
[52] D. Kanjilal, S. Chopra, M. M. Narayanan, Indira S. Iyer, Vandana Jha, R. Joshi, and S. K. Datta, Nucl. Instrum. Methods Phys. Res., Sect. A **328**, 97 (1993).
[53] A. K. Sinha, N. Madhavan, J. J. Das, P. Sugathan, D. O. Kataria, A. P. Patro, and G. K. Mehta, Nucl. Instrum. Methods Phys. Res., Sect. A **339**, 543 (1994).
[54] P. D. Shidling, N. Madhavan, V. S. Ramamurthy, S. Nath, N. M. Badiger, Santanu Pal, A. K. Sinha, A. Jhingan, S. Muralithar, P. Sugathan, S. Kailas, B. R. Behera, R. Singh, K. M. Varier, and M. C. Radhakrishna, Phys. Lett. B **670**, 99 (2008).
[55] S. Nath *et al.*, Phys. Rev. C **81**, 064601 (2010); Nucl. Phys. A **850**, 22 (2011).
[56] S. Nath, Comput. Phys. Commun. **180**, 2392 (2009).
[57] A. Gavron, Phys. Rev. C **21**, 230 (1980); http://lise.nscl.msu.edu/5_13/lise_5_13.html
[58] V. Zanganeh, R. Gharaei, and N. Wang, Phys. Rev. C **95**, 034620 (2017).
[59] G. Montagnoli, A. M. Stefanini, L. Corradi, S. Courtin, E. Fioretto, F. Haas, D. Lebhertz, F. Scarlassara, R. Silvestri, and S. Szilner, Phys. Rev. C **82**, 064609 (2010).
[60] K. Hagino, T. Takehi, A. B. Balantekin, and N. Takigawa, Phys. Rev. C **71**, 044612 (2005).
[61] J. O. Newton, R. D. Butt, M. Dasgupta, D. J. Hinde, I. I. Gontchar, C. R. Morton, and K. Hagino, Phys. Lett. B **586**, 219 (2004).
[62] E. Martínez-Quiroz, E. F. Aguilera, J. J. Kolata, and M. Zahar, Phys. Rev. C **63**, 054611 (2001).
[63] P. Moller, R. Nix, W. D. Mayers, and W. J. Swiatecki, At. Data Nucl. Data Tables **59**, 185 (1995).
[64] A. M. Stefanini, D. Ackermann, L. Corradi, D. R. Napoli, C. Petrache, P. Spolaore, P. Bednarczyk, H. Q. Zhang, S. Beghini, G. Montagnoli, L. Mueller, F. Scarlassara, G. F. Segato, F. Soramel, and N. Rowley, Phys. Rev. Lett. **74**, 864 (1995).
[65] H. Timmers, L. Corradi, A. M. Stefanini, D. Ackermann, J. H. He, S. Beghini, G. Montagnoli, F. Scarlassara, G. F. Segato, and N. Rowley, Phys. Lett. B **399**, 35 (1997).
[66] S. E. Woosley *et al.*, At. Data Nucl. Data Tables **22**, 371 (1978).
[67] C. L. Jiang, K. E. Rehm, R. V. F. Janssens, H. Esbensen, I. Ahmad, B. B. Back, P. Collon, C. N. Davids, J. P. Greene, D. J. Henderson, G. Mukherjee, R. C. Pardo, M. Paul, T. O. Pennington, D. Seweryniak, S. Sinha, and Z. Zhou, Phys. Rev. Lett. **93**, 012701 (2004).
[68] J. J. Vega, E. F. Aguilera, G. Murillo, J. J. Kolata, A. Morsad, and X. J. Kong, Phys. Rev. C **42**, 947 (1990).